New Second-Order Polytropic Numerical Model for Stirling Cycle Heat Pump

Temesgen Assefa Minale[a,b], François Lanzetta[a], Sylvie Bégot[a], Muluken Zegeye Getie[b], Steve Djetel-Gothe[a]

[a] *Université Marie et Louis Pasteur, CNRS, institut FEMTO-ST, F-90000 Belfort, France*
[b] *Faculty of Mechanical and Industrial Engineering, Bahir Dar Institute of Technology, Bahir Dar University, Bahir Dar, Ethiopia*

Abstract

Any machine design needs an understanding of the procedures that determine the operating principles and governing equations of the system. This understanding is necessary to investigate the behavior of the system and to draw an estimate of performance. In this paper, a new second-order numerical model was developed to predict the performance of the Stirling cycle heat pump. The governing differential equation of the Stirling heat pump has been developed by coupling the effect of polytropic heat transfer, shuttle heat loss, and mass leakage to buffer space and into the two working spaces. The proposed numerical modeling is simulated using MATLAB software. The model has been experimentally validated by converting the existing FEMTO-60 engine into a heat pump. In addition, this model is validated by changing the governing equation in an engine model accordingly. The newly developed numerical model predicted performance COP of 0.9, 1.2, and 1.6 with a relative error of 1.1 %, 9.0 %, and 14.3 % at frequencies of 12.1 Hz, 9.7 Hz, and 7.3 Hz, respectively, for nitrogen gas at a working pressure of 17.5 bar.

Keywords: Stirling heat pump, Power loss, Work loss, Heating capacity, Coefficient of performance

1. Introduction

Researchers and governments are looking for alternative heating and cooling solutions as a result of growing concerns about climate change. Due to this climate concern, Stirling heat pumps are positioned as a key technology for the net-zero agenda in the future. Stirling heat pumps are a promising heating technology for residential and commercial applications because of their natural working fluids. Beale reported that Stirling cycle devices could be used as an engine and heat pump [7]. The device used as a refrigerator

or heat pump, which is the reverse process of the Stirling engine, was first developed in 1832 [20].

Nomenclature

General

A Area [m^2]
C Average molecular speed [$m.s^{-1}$]
C_p Specific heat at constant pressure [$J.kg^{-1}.K^{-1}$]
C_v Specific heat at constant volume [$J.kg^{-1}.K^{-1}$]
d Diameter [m]
f Frequency [Hz]
f_r Friction factor
G Mass flux [$kg.m^{-2}.s^{-1}$]
h Convective heat transfer coefficient [$W.m^{-2}.K^{-1}$]
K Material Thermal conductivity [$W.m^{-1}.K^{-1}$]
L Length [m]
M Mass [Kg]
n Number
NTU Number of Transfer Unit
Nu Nusselt number
P Pressure [Pa]
P_r Prandtl number
p Piston
Q Quantity of heat [J]
R Gas constant [$J.kg^{-1}.K^{-1}$]
R_e Reynolds number
s Stroke [m]
T Temperature [K]
U Piston speed [$m.s^{-1}$]
V Volume [m^3]
W Work [J]

Greek Symbols

Δ Change
γ Ratio of specific heats
μ Gas dynamic viscosity [$kg.m^{-1}.s^{-1}$]
ϕ Porosity
ρ Density [$kg.m^{-3}$]
τ Compression ratio
θ Crank angle [°]
ω Angular frequency [$rad.s^{-1}$]
ε Effectiveness of regenerator

Subscripts

act Actual
c Compression space
ce Compression-expansion space interface
ch Compression space-heater interface
$cond$ Conduction
$disp$ Dissipation
e Expansion space
fs Finite speed
h Heater
hr Heater-regenerator interface
hy Hydraulic
$hyst$ Hysteresis
ke Cooler-expansion space interface
k Cooler
$leak$ Leakage
m Mesh
mf Mechanical friction
r Regenerator
rk Regenerator-cooler interface
wh Wall of heater
wk Wall of cooler
w Wire
SW Swept volume

The Stirling cycle heat pump device is called a regenerative thermal device due to the presence of the regenerator. This helps to reduce the energy

demand in the heating and cooling effect of the device. The detailed technological development of the Stirling cycle heat pump has been conducted in the study [26].In the study, the working principles, energy consumption in residential and commercial buildings, driving mechanisms and configuration of Stirling cycle heat pumps have been studied. Furthermore, the development of thermodynamic or numerical modeling techniques applied to Stirling cycle devices has been conducted in the study [27]. In this study, the authors discuss the existing numerical model and compare each model with the experimental value of the GPU3 engine.

There are typically three forms of loss in a Stirling machine analysis. The differential equation took into account gas leakage and shuttle heat loss, and polytropic heat loss as the first category of losses. To adjust the temperature of the Stirling machine, second-category losses, including non-ideal heat transfer, pumping loss, conduction heat loss, and radiation heat loss, were analysed alongside first-category losses.. The pressure drop or fluid friction loss, spring hysteresis loss, mechanical friction between the piston and displacer, and pressure loss resulting from the finite speed were all computed as distinct loss factors for the third category of losses, which had no impact on temperature distribution and were considered an independent loss [5]. Hence, the effect of the third category losses is considered to correct the performance of the heat pump (work input, COP, and heating power). The previous studies [5, 4, 16, 17, 31] for numerical modeling of Stirling machines consider the thermal and power loss in the energy and mass equations.

To enhance the second-order numerical modeling of Stirling cycle devices, a new polytropic and adiabatic model with a variety of losses has been developed [4, 5, 31]. The new non-ideal second-order thermal model with additional loss effects was the best numerical model among the existing numerical models [31]. In this work, a new second-order polytropic numerical model was developed by modifying the previous thermal models[31] with the working space considered as a polytropic process. Although this model predicted a better prediction, it did not consider the radiation loss, pumping loss, and polytropic heat transfer loss in the working spaces.

Therefore, the new second-order polytropic model has been formulated by including those losses. The differential energy conservation equation is changed to include polytropic heat loss, shuttle heat loss, and mass leakage loss to working space, which leads to modifying the pressure equation. The new set of differential equations was numerically solved by using 4^{th} order Runge-Kutta method. The numerical solution's result was then adjusted by non-ideal heat transfer in heat exchangers, internal heat conduction loss, heat dissipation loss, radiation heat loss, and pumping heat loss. Mechanical friction between the piston and displacer, spring hysteresis loss, pressure drop work loss in heat exchangers, and the finite speed work loss were all taken into account in the work input modification. The reverse process of the FEMTO-60 Stirling engine was used as a case study for the simulation

and experimental validation of the model. Therefore, the performance of a Stirling heat pump could be accurately predicted by the newly developed numerical model.

2. Numerical modeling

2.1. Ideal Adiabatic model

The set of equations that govern the Stirling cycle heat pump for an ideal adiabatic model is summarized in Table 1. This set of equations is developed by taking the assumption formulated by [33].

Table 1: Ideal adiabatic set of equations [14].

Parameter	Equation
Pressure	$P = \frac{mR}{\frac{V_c}{T_c}+\frac{V_h}{T_h}+\frac{V_r}{T_r}+\frac{V_k}{T_k}+\frac{V_e}{T_e}}$
Variation of pressure	$dP = \frac{-P\gamma(\frac{dV_c}{T_{ck}}+\frac{dV_e}{T_{ke}})}{\frac{V_c}{T_{ck}}+\gamma(\frac{V_h}{T_h}+\frac{V_r}{T_r}+\frac{V_k}{T_k})+\frac{V_e}{T_{ke}}}$
Mass	$m_i = \frac{PV_i}{RT_i}$, where (i = c, h, r, k, e)
Accumulation of mass	$dm_i = \frac{m_i dP}{P} = \frac{dP_i}{R}\frac{V_i}{T_i}$, where (i=h, r, k) $dm_c = \frac{PdV_c+\frac{V_c dP}{\gamma}}{RT_{ch}}$ $dm_e = \frac{PDV_e+\frac{V_e DP}{\gamma}}{RT_{ke}}$
Mass flow	$\dot{m}_{ch} = -dm_c$ $\dot{m}_{ke} = -dm_e$ $\dot{m}_{hr} = \dot{m}_{ch} - dm_h$ $\dot{m}_{rk} = \dot{m}_{ke} - dm_k$
Conditional Temperature	If $\dot{m}_{ch} > 0, then T_{ch} = T_c, else, T_{ch} = T_h$ $\dot{m}_{ke} > 0, then T_{ke} = T_k, else T_{ke} = T_e$
Variation of Temperature	$dT_e = T_e(\frac{dP}{P} + \frac{dV_e}{V_e} - \frac{dm_e}{m_e})$ $dT_c = T_c(\frac{dP}{P} + \frac{dV_c}{V_c} - \frac{dm_c}{m_c})$
Energy power	$dQ_h = (V_h dPC_v)/R - C_p(T_{ch}\dot{m}_{ch} - T_{hr}\dot{m}_{hr})$ $dQ_r = (V_r dPC_v)/R - C_p(T_{hr}\dot{m}_{hr} - T_{rk}\dot{m}_{rk})$ $dQ_k = (V_k dPC_v)/R - C_p(T_{rk}\dot{m}_{rk} - T_{ke}\dot{m}_{ke})$ $dW_{in} = -(dW_C + dW_{e)}$ where $dW_C = PdV_C, and, dW_e = PdV_e$

2.2. New second-order polytropic model

The performance predicted by the ideal adiabatic model is far from the experimental result due to its ideal assumption, and there is no consideration of power and work loss, which are discussed in Section 2.3.

The polytropic model is a second-order numerical model method in which the compression and expansion space of the heat pump compartment is considered a polytropic process instead of the adiabatic process. Similarly as the ideal adiabatic model, the overall heat pump machine is divided into five serially connected control volumes. It consists of compression space (c), heater(h), regenerator(r), cooler (k), and expansion space(e), respectively, see Fig 1. The properties of the working fluid in the Stirling heat pump are represented by its mass (m), temperature (T), volume (V), and pressure (p).

The two working spaces are assumed to be polytropic processes, and the temperatures T_c and T_e vary over the cycle. Work is done on the system by virtue of varying the volume of working spaces V_c and V_e.The heat Q_h and Q_k are the heat transfer between the environment and working fluid in the heater and cooler, respectively, and Q_r is the internal heat transfer between the gas and regenerator matrix. There are four interfaces through which enthalpy is transported by mass flow $\dot{m}$. These are the compression space-heater (ch), heater-regenerator (hr), regenerator-cooler (rk), and cooler-expansion space (ke). There is also one additional interface between the compression-expansion space (ce) due to mass leakage (Fig. 1).

The governing equation of the control volume is based on the state equation and the principles of conservation of energy and mass. By ignoring the change in potential and kinetic energy, the energy equation for the control volume can be written as follows (Fig. 2). The suffix x represents the polytropic loss, heat dissipation loss, shuttle loss, conduction loss, non-ideal regenerator loss, and leakage loss.

$$Q_x + C_p(m_i T_i + m_o T_o) = dW_{ideal} + dW_{fs} + dW_{mf} + dW_{pd} + dW_{hys} + C_v d(mT) \tag{1}$$

Where dW_{ideal}, C_p, and C_v are the ideal work loss, ideal work input, and specific heat capacity at constant pressure and volume, respectively. The losses dW_{fs}, dW_{mf}, W_{pd}, and dW_{hys} are the additional work loss by finite speed of piston, mechanical friction of the piston and displacer, pressure drop, and spring hysteresis, respectively.

The total mass of the working fluid in the Stirling heat pump is not constant because of the leakage of the working fluid into the crankcase. Thus, using this information as a basis, the following formulas can be used to calculate the total mass of the working fluid in the heat pump.

$$m_t = M - m_{leak} = m_c + m_h + m_r + m_k + m_e - m_{leak} \tag{2}$$

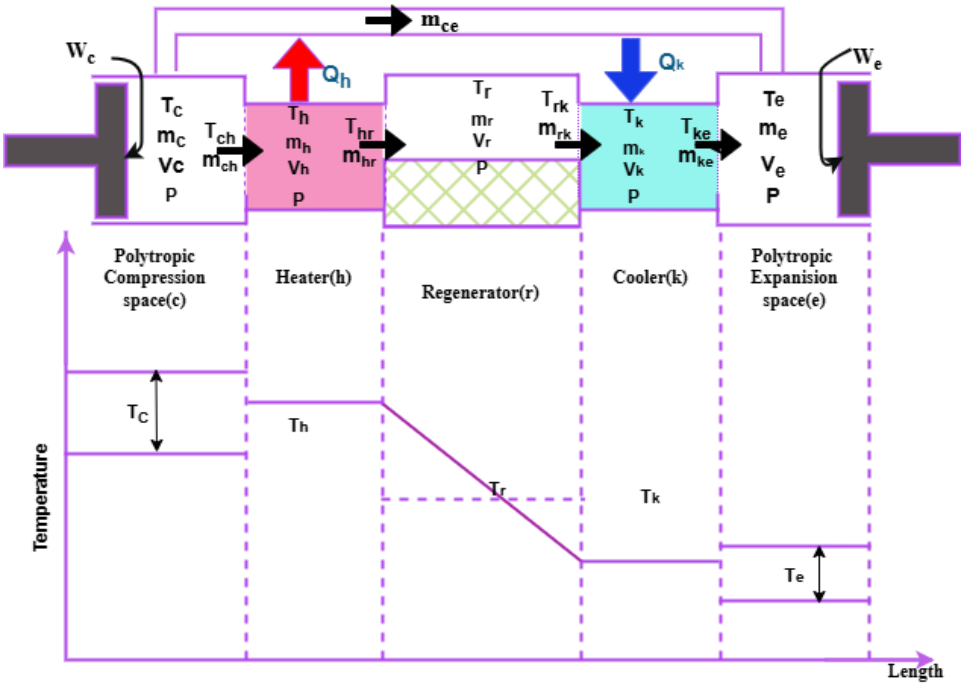

Figure 1: Polytropic model with mass leakage to working space

In addition, the differential form of this total mass equation can be written as:

$$dm_c + dm_h + dm_r + dm_k + dm_e - dm_{leak} = 0 \tag{3}$$

Where dm_{leak} is the mass of the leakage working fluid into the crankcase of the heat pump, and the rate of this term is expressed as follows [33]:

$$\dot{m}_{leak} = \pi d_p \frac{P + P_{buffer}}{4RT_g}(U_P J - \frac{J^3}{6\mu L_P}(P - P_{buffer})) \tag{4}$$

where $L_P, d_P, U_P, T_g, \mu, R, J, P$ and P_{buffer} are length of piston, diameter of piston, linear velocity of piston, temperature of the gas, viscosity of the fluid, gas constant of the fluid, the annular gap between the cylinder wall and piston, working space pressure, and buffer pressure, respectively.

Applying the energy equation for a compression space control volume based on equation (1), we obtain:

$$-dQ_{poly} - dQ_{shut} - C_p T_{ch} dm_{ch} - C_p T_{ce} dm_{ce} = dW_c + C_v d(mT) \tag{5}$$

The expansion and compression spaces are maintained at different temperature levels, and the displacer moves from the cold space to the hot space or

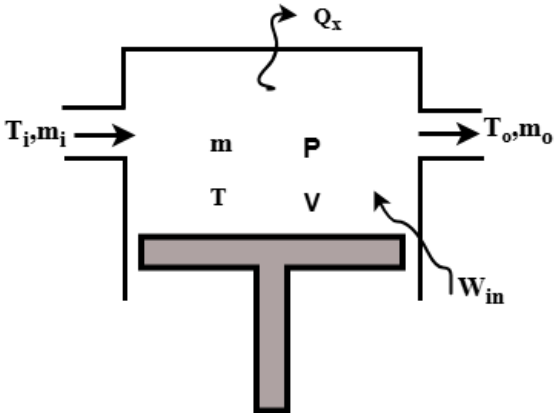

Figure 2: Control volume of the heat pump section

vice versa. This displacement motion results in a loss or gain of heat between the two working spaces. The amount of heat gained or lost by this displacer is known as shuttle heat loss. This has been determined by [25, 30]:

$$dQ_{shut} = \frac{\pi s^2 k_g d_d}{8JL_d}(T_c - T_e) \tag{6}$$

Where s, k_g, d_p, J, L_d, T_c, and T_e are the displacer stroke, thermal conductivity, piston diameter, annular gap between displacer and cylinder wall, piston length, gas temperature in compression and expansion, respectively.

The polytropic heat transfer loss from the heat pump to the surrounding area is Q_{poly} modeled by [35, 5]:

$$Q_{poly} = mC_n(T_a - T) \tag{7}$$

Differentiating equation 7, we obtain

$$dQ_{poly} = C_n(T_a - T)dm - mC_n dT \tag{8}$$

Where m, C_n, T_a, T are mass, polytropic specific heat capacity, ambient, and working space temperature, respectively. The polytropic specific heat capacity is calculated as follows [24]:

$$C_n = C_v \frac{n-k}{n-1} \tag{9}$$

Where n is the polytropic index and calculated by the following equation:

$$PV^n = constant \tag{10}$$

Differentiating the equation to obtain the polytropic index of the gas in the

two working spaces.

$$n = \frac{VdP}{PdV} \tag{11}$$

Where V, dV, p, and dp are the volume, differential volume, pressure, and differential pressure, respectively. The pressure and differential pressure are calculated based on an equation in Table 2. Volume and differential volume are calculated based on the sinusoidal volume variation as a function of the crank angle [33].

Due to mass leakage by the displacer, there is a drop in enthalpy in the hot working space, which leads to a gain in enthalpy in the cold working space. This loss is due to mass leakage to the working space and is modeled by the equation [15, 22]:

$$\dot{m}_{ce} = \pi d_d \frac{P}{4RT_{ce}}(U_d J - \frac{J^3}{6\mu L_d}(\Delta p_{ce})) \tag{12}$$

Where U_d, T_{ce}, and ΔP_{ce} are the displacer velocity, the temperature of the leakage fluid, and the pressure difference between the hot and cold working spaces, respectively.

The conservation of mass has been applied to each control volume for obtaining the mass flow rate of the working fluid as follows:

$$dm_{Ch} = -dm_c - dm_{ce} \tag{13}$$

$$dm_{hr} = dm_{Ch} - dm_h \tag{14}$$

$$dm_{rk} = dm_{hr} - m_r \tag{15}$$

$$dm_{ke} = dm_{rk} - dm_k \tag{16}$$

$$dm_e = dm_{ke} + m_{ce} \tag{17}$$

Therefore, by substituting equation (8) in equation (5), we obtain the following equation for two working spaces:

$$-C_n(T_a - T)dm + mC_n dT - dQ_{shut} - C_p T_{ch} dm_{ch} - C_p T_c e dm_{ce} = dW + C_v d(mT) \tag{18}$$

Applying the state equation of an ideal gas in equation 18 and $dW = PdV_c$, the energy balance equation for the compression space can be written as:

$$C_n(T_c - T_a)dm_c + m_c C_n dT_c - dQ_{shut} - C_p T_{ch} dm_{ch} - C_p T_{ce} dm_{ce} = dW_c + C_v d(m_c T_c) \tag{19}$$

$$C_n(T_c - T_a)dm_c + m_c C_n dT_c - dQ_{shut} - C_p T_{ch} dm_{ch} - C_p T_{ce} dm_{ce} = PdV_c + C_v d(\frac{PV_c}{R}) \tag{20}$$

By simplifying equation 20, the differential mass flow rate for the compression space can be written as:

$$dm_c = \frac{\frac{PdV_c + \frac{V_c dP}{\gamma}}{RT_{ch}} + \frac{C_n}{C_p}\frac{m_c}{T_{ch}}dT_c + \frac{dQ_{shut}}{c_p T_{ch}} + \frac{T_{ce}dm_{ce}}{T_{ch}} - dm_{ce}}{[\frac{C_n}{C_p}(\frac{T_c - T_a}{T_{ch}}) + 1]} \tag{21}$$

Similarly, the differential mass flow rate for the expansion space can be written as:

$$dm_e = \frac{\frac{PdV_e + \frac{V_e dP}{\gamma}}{RT_{ke}} + \frac{C_n}{C_p}\frac{m_e}{T_{ke}}dT_e - \frac{dQ_{shut}}{c_p T_{ke}} - \frac{T_{ce}dm_{ce}}{T_{ke}} + dm_{ce}}{[\frac{C_n}{C_p}(\frac{T_c - T_a}{T_{ke}}) + 1]} \tag{22}$$

The equation of state for an ideal gas

$$PV = mRT \tag{23}$$

By differentiating equation (23), it can be written as:

$$\frac{dP}{P} + \frac{dV}{V} = \frac{dm}{m} + \frac{dT}{T} \tag{24}$$

For the three heat exchangers (heater, cooler, and regenerator), the term $DV/V = 0$, and we assume isothermal conditions, then equation (24) can be written as:

$$\frac{dP}{P} = \frac{dm}{m} \tag{25}$$

Then the change in mass in the three-heat exchanger becomes:

$$dm_i = m_i \frac{dP}{P} = \frac{V_i dP}{RT_i}(where, i = h, r, k) \tag{26}$$

Substituting equation (26) into equation (3), we obtain an equation:

$$dm_c + dm_e - \dot{m}_{leak} + \frac{dP}{R}(\frac{V_h}{T_h} + \frac{V_r}{T_r} + \frac{V_k}{T_k}) = 0 \tag{27}$$

Substituting equations (21) and (22) into equation (27), we obtain the following equation:

$$\begin{aligned} &\left[\frac{\frac{PdV_c + \frac{V_c dP}{\gamma}}{RT_{ch}} + \frac{C_n}{C_p}\frac{m_c}{T_{ch}}dT_c + \frac{dQ_{shut}}{c_p T_{ch}} + \frac{T_{ce}dm_{ce}}{T_{ch}} - dm_{ce}}{\left[\frac{C_n}{C_p}(\frac{T_c - T_a}{T_{ch}}) + 1\right]}\right] \\ &+ \left[\frac{\frac{PdV_e + \frac{V_e dP}{\gamma}}{RT_{ke}} + \frac{C_n}{C_p}\frac{m_e}{T_{ke}}dT_e + \frac{dQ_{shut}}{c_p T_{ke}} + \frac{T_{ce}dm_{ce}}{T_{ke}} - dm_{ce}}{\left[\frac{C_n}{C_p}(\frac{T_c - T_a}{T_{ke}}) + 1\right]}\right] \\ &-\dot{m}_{leak} + \frac{dP}{R}\left[\frac{V_h}{T_h} + \frac{V_r}{T_r} + \frac{V_k}{T_k}\right] = 0 \end{aligned} \tag{28}$$

By simplifying equation 28, the differential pressure dP can be written as:

$$\begin{aligned} dP = &-\gamma\left[\frac{\frac{PdV_c}{T_{ch}} + \frac{RC_n}{C_p}\frac{m_c}{T_{ch}}dT_c + \frac{RQ_{\text{shut}}}{C_p T_{ch}} + \frac{RT_{ce}\,dm_{ce}}{T_{ch}} - \frac{Rdm_{ce}}{T_{ch}}}{\frac{V_c}{T_{ch}} + \frac{V_e}{T_{ke}}\frac{A_1}{A_2} + A_1\gamma\left[\frac{V_h}{T_h} + \frac{V_r}{T_r} + \frac{V_k}{T_k}\right]}\right] \\ &-\gamma\left[\frac{\frac{PdV_e}{T_{ke}} + \frac{RC_n}{C_p}\frac{m_e}{T_{ke}}dT_e - \frac{RQ_{\text{shut}}}{C_p T_{ke}} - \frac{RT_{ce}\,dm_{ce}}{T_{ke}} + \frac{Rdm_{ce}}{T_{ke}}}{\frac{A_2}{A_1}\frac{V_c}{T_{ch}} + \frac{V_e}{T_{ke}} + A_2\gamma\left[\frac{V_h}{T_h} + \frac{V_r}{T_r} + \frac{V_k}{T_k}\right]}\right] \\ &+\frac{R\dot{m}_{\text{leak}}}{\frac{V_c}{T_{ch}A_1} + \frac{V_e}{T_{ke}A_2} + \gamma\left[\frac{V_h}{T_h} + \frac{V_r}{T_r} + \frac{V_k}{T_k}\right]} \end{aligned} \tag{29}$$

Where $A_1 = \left[\frac{C_n}{C_p}\frac{T_c - T_a}{T_c h} + 1\right]$ and $A_2 = \left[\frac{C_n}{C_p}\frac{T_c - T_a}{T_{ke}} + 1\right]$

The temperature change in the two working spaces could be obtained by using equation (24) as follows:

$$dT_e = T_e(\frac{dP}{P} + \frac{dV_e}{V_e} - \frac{dm_e}{m_e}) \tag{30}$$

$$dT_c = T(\frac{dP}{P} + \frac{dV_c}{V_v} - \frac{dm_c}{m_c}) \tag{31}$$

Working fluid temperatures in compression and hot heat exchangers T_{ch}, coolers and expansion spaces T_{ke}, compression and expansion T_{ce} interfaces are conditional temperatures based on the flow direction and are calculated

as follows [33]:

$$If, \dot{m}_{ch} > 0, then, T_{ch} = T_c, else, T_{ch} = T_h \tag{32}$$

$$If, \dot{m}_{ke} > 0, then, T_{ke} = T_k, else, T_{ke} = T_e \tag{33}$$

$$If, \dot{m}_{ce} > 0, then, T_{ce} = T_k, else, T_{ce} = T_e \tag{34}$$

The heat transfer in the three heat exchangers (heater, regenerator, and cooler) could be calculated based on equation (1) and calculated as follows:

$$dQ_h = V_h \frac{dPC_v}{R} - C_p(T_{ch}\dot{m}_{ch} - T_{hr}\dot{m}_{hr}) \tag{35}$$

$$dQ_r = V_r \frac{dPC_v}{R} - C_p(T_{hr}\dot{m}_{hr} - T_{rk}\dot{m}_{rk}) \tag{36}$$

$$dQ_k = V_k \frac{dPC_v}{R} - C_p(T_{rk}\dot{m}_{rk} - T_{ke}\dot{m}_{ke}) \tag{37}$$

Table 2: Set of equations for the new polytropic model

Parameter	**Equation**
Pressure	$P = \frac{R(M - m_{\text{leak}})}{\frac{V_c}{T_c} + \frac{V_h}{T_h} + \frac{V_r}{T_r} + \frac{V_k}{T_k} + \frac{V_e}{T_e}}$
Pressure variation	$dP = \frac{-\gamma \left[\frac{\frac{PdV_c}{T_{ch}} + \frac{RC_n}{C_p} \frac{m_c}{T_{ch}} dT_c + \frac{RQ_{\text{shut}}}{C_p T_{ch}} + \frac{RT_{ce}\, dm_{ce}}{T_{ch}} - \frac{Rdm_{ce}}{T_{ch}}}{A_1} + \frac{\frac{PdV_e}{T_{ke}} + \frac{RC_n}{C_p} \frac{m_e}{T_{ke}} dT_e - \frac{RQ_{\text{shut}}}{C_p T_{ke}} - \frac{RT_{ce}\, dm_{ce}}{T_{ke}} + \frac{Rdm_{ce}}{T_{ke}}}{A_2} \right] + Rm_{\text{leak}}}{\frac{V_c}{T_{ch} A_1} + \frac{V_e}{T_{ke} A_2} + \gamma \left[\frac{V_h}{T_h} + \frac{V_r}{T_r} + \frac{V_k}{T_k} \right]}$ where $A_1 = \frac{C_n}{C_p} \frac{(T_c - T_a)}{T_{ch}} + 1$ and $A_2 = \frac{C_n}{C_p} \frac{(T_c - T_a)}{T_{ke}} + 1$
Mass	$m_i = \frac{PV_i}{RT_i}$ where $i = c, h, r, k,$ and e
Change of mass	$dm_i = m_i \frac{dP}{P} = \frac{V_i dP}{RT_i}$ where $i = h, r,$ and k $dm_c = \frac{\frac{PdV_c + \frac{V_c dP}{\gamma}}{RT_{ch}} + \frac{C_n}{C_p} \frac{m_c}{T_{ch}} dT_c + \frac{Q_{\text{shut}}}{C_p T_{ch}} + \frac{T_{ce} dm_{ce}}{T_{ch}} - dm_{ce}}{A_1}$ $dm_e = \frac{\frac{PdV_e + \frac{V_e dP}{\gamma}}{RT_{ke}} + \frac{C_n}{C_p} \frac{m_e}{T_{ke}} dT_e - \frac{Q_{\text{shut}}}{C_p T_{ke}} - \frac{T_{ce} dm_{ce}}{T_{ke}} + dm_{ce}}{A_2}$
Mass flow	$dm_{\text{ch}} = -dm_c - dm_{ce}$ $dm_{\text{hr}} = dm_{\text{Ch}} - dm_h$ $dm_{\text{rk}} = dm_{ke} + dm_h$ $dm_{ke} = dm_e - dm_{ce}$
Conditional temperature	If $\dot{m}_{ch} > 0$ then $T_{ch} = T_c$, else $T_{ch} = T_h$ If $\dot{m}_{ke} > 0$ then $T_{ke} = T_k$, else $T_{ke} = T_e$ If $\dot{m}_{ce} > 0$ then $T_{ce} = T_c$, else $T_{ce} = T_e$
Temperature variation	$dT_e = T_e \left(\frac{dP}{P} + \frac{dV_e}{V_e} - \frac{dm_e}{m_e} \right)$ $dT_c = T_c \left(\frac{dP}{P} + \frac{dV_c}{V_c} - \frac{dm_c}{m_c} \right)$
Polytropic index	$n_c = -\frac{V_c dP}{PdV_c}$ $n_e = -\frac{V_e dP}{PdV_e}$
Energy and power	$dQ_{h,\text{mp}} = \frac{V_h dP C_v}{R} - C_p(T_{ch}\dot{m}_{ch} - T_{hr}\dot{m}_{hr})$ $dQ_{r,\text{mp}} = \frac{V_r dP C_v}{R} - C_p(T_{hr}\dot{m}_{hr} - T_{rk}\dot{m}_{rk})$ $dQ_{k,\text{mp}} = \frac{V_k dP C_v}{R} - C_p(T_{rk}\dot{m}_{rk} - T_{ke}\dot{m}_{ke})$ $dW_{\text{in,mp}} = -(dW_C + dW_e)$ where $dW_C = PdV_C$ and $dW_e = PdV_e$

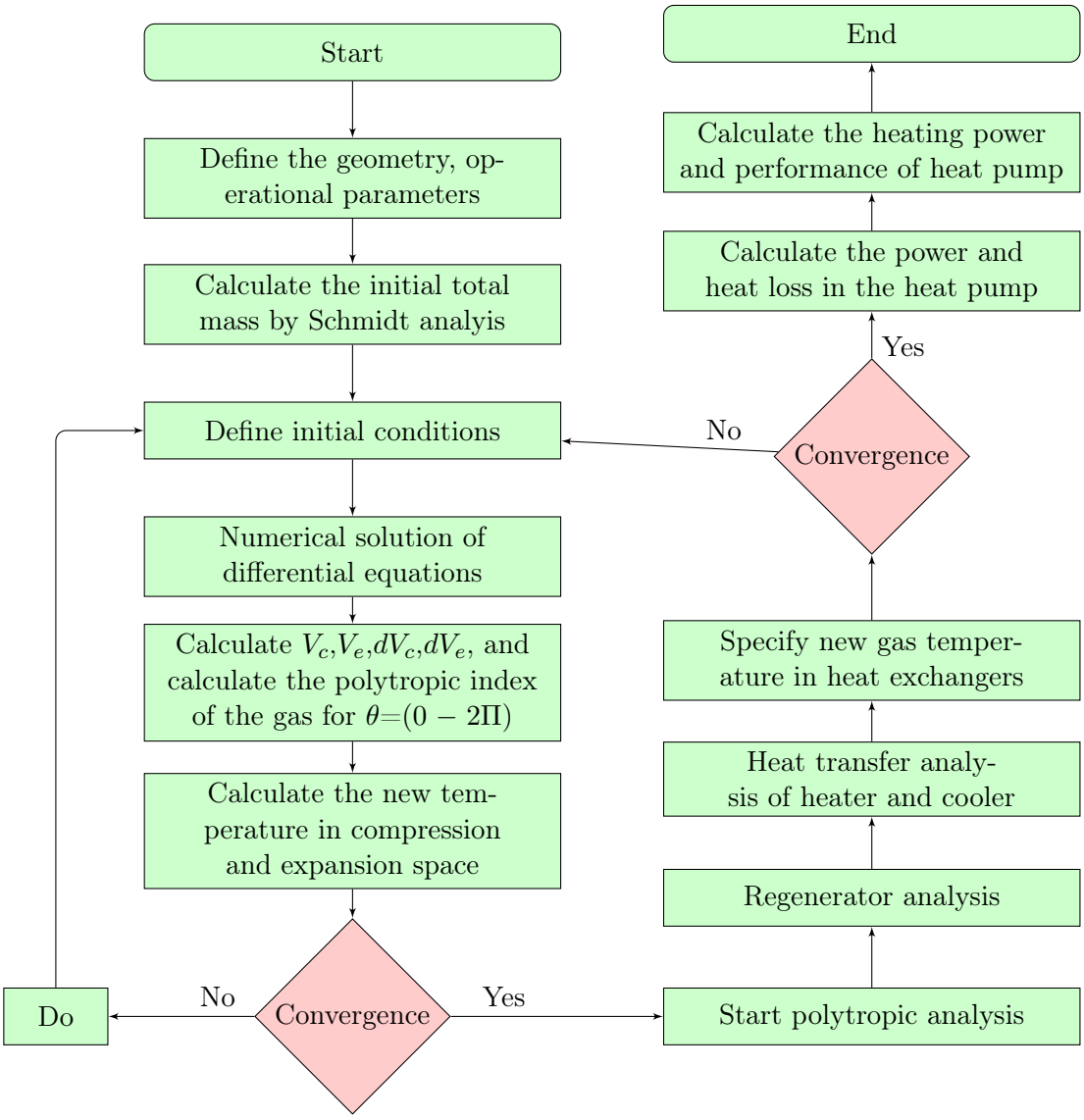

Figure 3: Flow diagram for new polytropic model of Stirling cycle heat pump

2.3. Second and third category loss in heat pump

The new polytropic model developed in this study was enhanced by considering the second and third-category losses of the heat pump at the end of each cycle for computational iteration. The third category of losses is work losses in the Stirling heat pump, which affect the power input for the heat pump, including mechanical friction loss, piston finite speed work loss, pressure drop work loss in the heat exchanger, and gas spring hysteresis loss. The second category of losses is heat losses, used to adjust the temperature

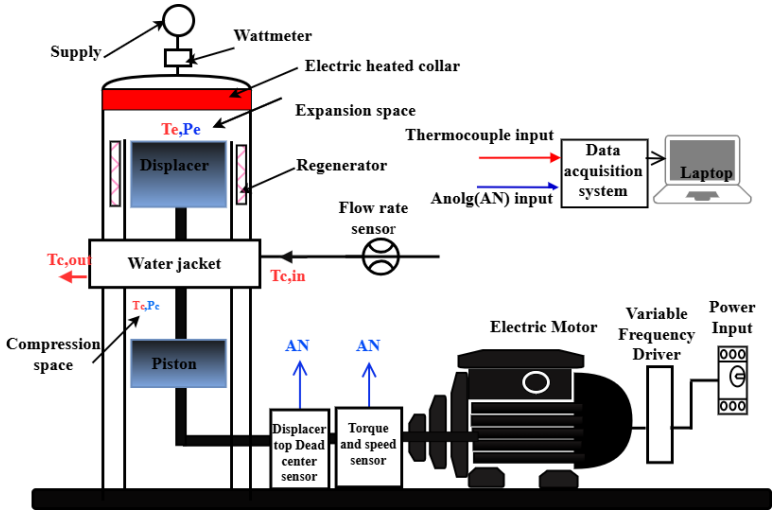

Figure 4: Experimental setup for model validation

of the working fluid at the end of the cycle, including conduction heat loss, dissipation heat loss, regenerator imperfection loss, leakage heat loss, pumping heat loss, and radiation heat loss. This section describes the methods for evaluating the second-category (power or heat loss) and third-category (work loss) losses in the Stirling heat pump.

2.3.1. Internal heat Conduction heat loss

In Stirling machines, there is a temperature variation across each heat exchanger compartment. This temperature variation leads to thermal energy loss through conduction. In particular, a considerable amount of heat is lost between the heater and cooler heat exchangers. This loss has been modelled using the following equation:[23, 29]:

$$Q_{cond} = \frac{kA(T_{wh} - T_{wk})}{Lf} \tag{38}$$

where k, A, f, L, T_{wh}, and T_{wk} are the thermal conductivity, area, frequency, length, heater wall temperature, and cooler wall temperature, respectively.

2.3.2. Dissipation heat loss

The thermal boundary layer is created due to the flow of the working fluid over the surface of the heat exchanger. This leads to dissipation heat loss, and this loss has been modeled by the equation below:

$$Q_{idisp} = \frac{m_i \Delta p}{\rho} \tag{39}$$

Where ρ and Δp are the density of the working fluid and the pressure change in the heat exchangers.

2.3.3. Non-ideal (regenerator imperfection) heat loss

A regenerator is designed to absorb heat from the working fluid during the process of constant-volume heat addition, and ideally release the same amount of heat to the working fluid during the process of constant-volume heat rejection. However, it is impossible to recover all the absorbed heat due to the regenerator's imperfections, which are evaluated by its effectiveness. Effectiveness is the ratio of the actual enthalpy of the gas passing through the regenerator to the theoretical maximum enthalpy change, and its value is between zero and one [33]. When the working fluid moves from the cooler to the heater in a Stirling heat pump with an imperfect regenerator, the temperature of the fluid as it leaves the regenerator will be somewhat lower than that of the heater. As a result, the heater provides additional heat to increase the temperature of the working fluid. The imperfection of the regenerator is defined based on the Number of Transfer Units (NTU) and expressed as:

$$\epsilon = \frac{NTU}{NTU + 1} \tag{40}$$

The Nusselt number (Nu) of the regenerator matrix is used to express the NTU, which is expressed as [2]:

$$NTU = \frac{L_r}{d_h} \frac{4NU}{R_e P_r} \tag{41}$$

Where L_r, d_h, R_e, P_r are regenerator length, regenerator hydraulic diameter, Reynolds and Prandtl number, respectively, and the hydraulic diameter is calculated by:

$$d_h = \frac{4V_{void}}{A_{wetted}} \tag{42}$$

The Nusselt number for oscillating flow in the regenerator was proposed by Gedeon and Wood [13] as follows:

$$Nu = ((1 + 0.99(R_e P_r)^{0.66}))\phi^{1.79} \tag{43}$$

Where ϕ is the porosity of the wire in the regenerator, and it can be calculated as [1]

$$\phi = 1 - \frac{\Pi n_m d_w}{4} \tag{44}$$

Where n_m and d_w are the number of meshes per meter and wire diameter of the regenerator mesh, respectively.

The extra heat supplied by the heater to compensate for the regenerator imperfection is calculated by

$$Q_{non-ideal,r} = dQ_r(1-\epsilon) \tag{45}$$

To compute the actual heat load of the heater and cooler by adding thermal loss to the energy balance equation:

$$Q_{h,actual} = dQ_h + Q_{non-ideal,r} - Q_{cond} - Q_{disp,total} - Q_{leak} \tag{46}$$

$$Q_{k,actual} = dQ_k - Q_{non-ideal,r} + Q_{cond} + Q_{disp,total} + Q_{leak} \tag{47}$$

In the non-ideal heat exchanger, the wall temperature of the heat exchanger is greater than the fluid temperature, and from Newton's law of heating and cooling, the expression could be obtained:

$$Q_{h,actual} = \frac{h_h A_h (T_{wh} - T_h}{f} \tag{48}$$

$$Q_{k,actual} = \frac{h_k A_k (T_{wk} - T_k}{f} \tag{49}$$

Where $h_k, h_h, T_{wk}, T_{wh}, A_h, T_k, T_h$ and f are the cooler and heater heat transfer coefficients, heat exchanger wall temperature of cooler and heater, area of cooler and heater, cooler and heater temperature, and frequency, respectively. Equations (50) and (51) are used to update the temperature of the heater and cooler at the end of the cycle by using the equations:

$$T_h = T_{wh} - \frac{fQ_{h,actual}}{h_h A_h} \tag{50}$$

$$T_k = T_{wk} - \frac{fQ_{k,actual}}{h_k A_k} \tag{51}$$

The cooler and heater heat transfer coefficient could be obtained from the correlation as [22]

$$h_i = \frac{0.0791 \mu_i C_p R_{ei}^{0.75}}{2 d_{hi} P_{ri}} \tag{52}$$

2.3.4. Leakage heat loss to buffer space

There is some heat loss due to the leakage of the mass to the crankcase, and this loss affects the performance of the heat pump. The heat loss due to the mass leakage into the crankcase is modeled by the equation:

$$Q_{leak} = m_{leak} C_p T_C \tag{53}$$

2.3.5. Radiation heat loss

The displacer or hot cup of the heat pump is usually hollow. The heat loss across this space is caused by heat conduction and radiation heat transfer. The radiation heat transfer is modeled by an equation:

$$Q_r = F_a F_m F_n A \sigma (T_h^4 - T_k^4) \tag{54}$$

where F_a, F_m, F_n, A and σ are the area factor, emissivity factor, radiation shielded factor, area of the displacer, and Stefan-Boltzmann constants, respectively.

2.3.6. Pumping heat loss

The heat can be absorbed in the wall of the cylinder and transferred to the working fluid in the clearance space due to periodic variations of the pressure in the cycle. Therefore, this pumping loss is because of the clearance volume and leads to the cooling of the working fluid in the heat pump. This heat loss is modeled by an equation [11, 22]:

$$Q_p = \dot{m} C_p (T_c - T_e)(1 - \eta) \tag{55}$$

where

$$\dot{m} = P_a \frac{2 f d_d L_d J}{R(T_c + T_e)}, \text{ and } \eta = 1 - \frac{4 \dot{m}^{0.6} C_p^{0.6} J}{3 \Pi k_g^{0.6} L_d^{0.6} d_d} \tag{56}$$

2.3.7. Mechanical friction work loss

There is a relative motion between the rotating part of the heat pump and this motion leads to mechanical friction loss, which increases the power input requirement of the heat pump. The following equation is used to determine the power loss in one cycle as a result of mechanical friction [14]:

$$dW_{m.f} = 2 \Delta P_{m.f} V_{swc} \tag{57}$$

Where the pressure loss due to mechanical friction of the component per cycle is calculated as [9]:

$$\Delta P_{m.f} = \frac{10^5 (0.94 + 0.045 sf)}{3(1 - \frac{1}{3\tau})} (1 - \frac{1}{\tau}) \tag{58}$$

Where s, f, and τ are the stroke, frequency, and compression ratio, respectively.

2.3.8. Piston finite speed work loss

The working spaces are regularly compressed and expanded by the pistons, or piston and piston/displacer, in a regenerative Stirling cycle system. The instantaneous pressure in compression and expansion regions is different from the pressure in the corresponding piston surfaces, according to the finite speed thermodynamic principle. The product of pressure drops and piston swept volume is used to calculate the work losses resulting from the piston's finite speed in one cycle [9, 16, 21] expressed as:

$$dW_{fs} = 2\Delta P_{fs} V_{SWC} \tag{59}$$

$$\Delta P_{fs} = \frac{aP}{2}\left(\frac{U_{P,c}}{c_c} + \frac{U_{P,e}}{c_e}\right) \tag{60}$$

Where, P, U_P, and C are the instantaneous pressure, piston speed, and average molecular speed of the piston. The value of a and C obtained by:

$$a = \sqrt{3\gamma}, c = \sqrt{3RT} \tag{61}$$

2.3.9. Pressure drop work loss in heat exchanger

The internal flow of working fluid in the heater, regenerator, and cooler has direct contact with the wall of the heat exchangers. This contact leads to fluid friction loss or a pressure drop loss, which affects the performance of the heat pump. The pressure drop work loss in the heat exchanger is calculated as [14, 31]:

$$dW_{pdi} = \int_0^{360} (\Delta p \frac{dv}{d\theta}) d\theta_i, (i = h, r, k) \tag{62}$$

$$\Delta p = \frac{2 f_i u_i \mu_i V_i}{A_i d_{hi}^2}$$

Where f, u, V, and A are the friction factor, flow velocity, volume, and area of the heat exchanger, respectively. The friction factor (f) could be obtained from an empirical correlation based on the flow regime of the flowing fluid in the heat exchanger and the correlation given by [9] as follows:

$$f_{h,k} = \begin{cases} 16, & \text{if } \mathrm{Re} < 2000, \\ 7.343 \times 10^{-4}\,\mathrm{Re}^{1.3142}, & \text{if } 2000 \le \mathrm{Re} < 4000, \\ 0.0791\,\mathrm{Re}^{0.75}, & \text{if } \mathrm{Re} > 4000. \end{cases} \tag{63}$$

And the friction factor for a regenerator with a woven matrix by Kays and London [18] is expressed as:

$$f_r = 54 + 1.43Re^{0.78} \tag{64}$$

2.3.10. Gas spring hysteresis work loss

It's possible that the Stirling machine's internal gas will start to operate like a spring when it is regularly compressed and expanded by the piston or displacer. The internal energy of the working fluid may be wasted in the Stirling machine because of this thermodynamic process, which is not recovered and may cause additional losses. When the working gas is compressed, it acts like a gas spring, storing energy and releasing it when it is expanded. This loss of energy is modeled by the following equation [33].

$$dW_{shyst} = (\frac{V_{swd}}{2V_t})^2 \frac{A_w}{4} \sqrt{\frac{1}{2}\omega\gamma^3(\gamma-1)kT_wP_{mean}} \tag{65}$$

Where $V_{swd}, V_t, A_w, \omega, k, T_w$ and P_{mean} are the swept volume of displacer, average total volume, wetted area of piston, angular velocity of piston, thermal conductivity of the gas, chamber wall temperature and mean pressure in the, pump respectively.

Therefore, the coefficient of performance of the hat pump has been obtained by adding the work loss from the ideal work input and subtracting the heat loss from the ideal heat gain in the heater as:

$$dW_{actul} = dW_{ideal} + dW_{shyst} + dW_{pdi} + dW_{fs} + dW_{m.f} \tag{66}$$

Therefore, the performance of the heat pump is obtained as:

$$COP_{hp} = \frac{dQ_{h,actual}}{dW_{actul}} \tag{67}$$

3. Solution method

The numerical model developed in Table 2 is a set of differential equations that govern the properties of the heat pump. A numerical algorithm method was developed for obtaining the solution of a differential equation. As can be seen from the flow diagram, the first step starts with defining the geometry and operational parameters of the engine. The specific engine configuration and geometry define V_e, V_C, dV_e and dV_C a functions of crank angle θ. The void volumes are V_h, V_r, V_k obtained from the geometry of heat exchangers. The parameters γ, R, C_p and C_v are determined from the choice of the working fluid. The value of T_h, T_k determined from the operating parameters of the engine, which are the initial temperature of the working

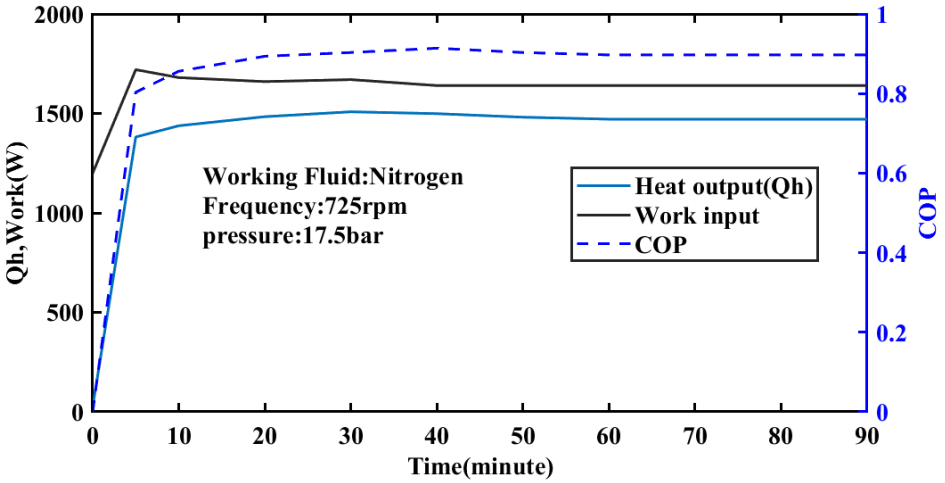

Figure 5: Variation of heat output and work input with respect to time

fluid in the hot and cold heat exchangers, respectively. The gas temperature in the regenerator is determined from the mean effective temperature (T_r) of the heater and cooler temperatures [13]. The initial mass of the working fluid in the control volume is determined from the Schmidt analysis by using the mean operating pressure from the operating condition.

We have seen that, except for the above constant parameters, there are 26 variables and 19 derivatives in the equation set to be solved over a complete cycle, 0 to 360 degrees. The seven derivative parameters T_c, T_e, Q_h, Q_r Q_k, W_c, W_e solved by the fourth-order Runge-Kuta method. Twelve analytical and derivative parameters $Q_{shutle}, m_{leak}, m_{ce}, W, P, V_e, V_C, m_c, m_h, m_h, m_h$ and m_h solved analytically. The other seven parameters $T_{ce}, T_{ch}, T_{ke}, m_{ch}, m_{hr}$ m_{rk}, and m_{ke} are conditional temperature and mass flow variables.

4. Model Validation and experimental setup

The model validation for the new numerical model developed for Stirling heat pumps can be validated experimentally or by previous research. Due to the lack of previous research on the Stirling heat pump modeling techniques, the new numerical model developed was validated by the FEMTO-60 engine that operates as a heat pump device by converting the process.

The experimental setup of the device is shown in Fig.4 and is the same as [12]. The mean pressure and temperature in the compression and expansion spaces are measured by pressure transducers and K-type thermocouples, respectively. The geometrical and parametric specification of the Stirling device, used for validation of the model, is shown in Table 3.

This numerical model was validated at frequencies of 7.3, 9.7, and 12.1 Hz for a series of heating and 17.5 bar charging pressures using nitrogen as

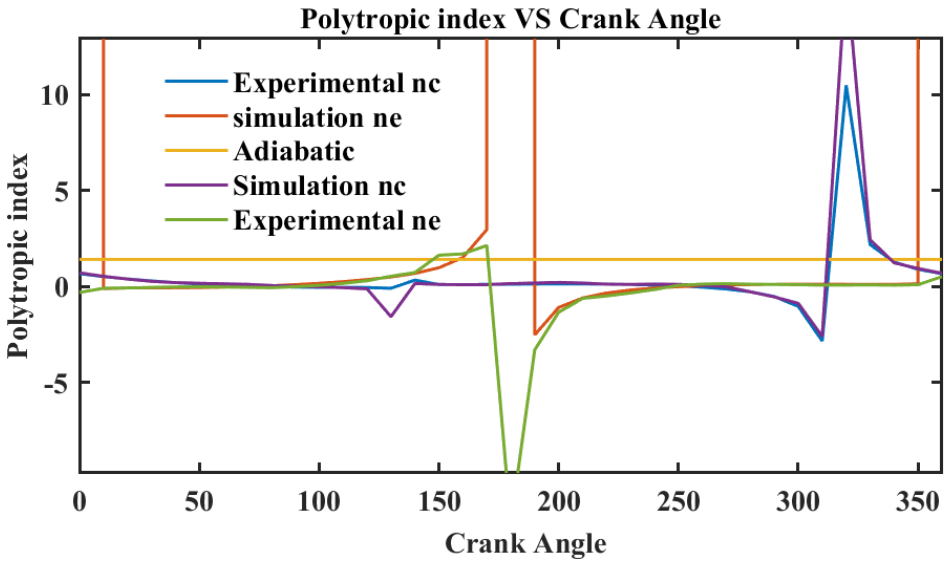

Figure 6: Variation of polytropic index with respect to crank angle

a working fluid.

Another approach is to adopt the geometry of the GPU-3 Stirling engine and modify the governing equations accordingly, enabling a comparison between numerical results and experimental data from the GPU-3 engine. Table 4 presents the validation of the current numerical model(new second-order polytropic model for the Stirling cycle heat pump) when applied as an engine model. The results indicate that this model yields the closest agreement with the experimental performance of GPU-3 engines operating with helium at a heater temperature of 977 K, cooler temperature of 288 K, charging pressure of 4.14 MPa, and frequency of 41.67 Hz. This confirms that the model can accurately predict the heat pump's performance.

5. Result and discussion

The operating parameters and geometry of the Stirling cycle heat pump, which is the reverse process of the FEMTO-60 engine, are listed in Table 3. The effect of polytropic heat transfer, shuttle heat loss, and mass leakage on the working space in the differential equation is analyzed.

Figure 5 shows how the heat output, work input, and COP of the heat pump vary over time, at 725 rpm and a working pressure of 17.5 bar, using nitrogen gas. As shown in the figure, the heat absorber starts to absorb heat, and the heat pump approaches a steady state after 10 minutes. The work input increases from 1200 to 1640 W, and the heat output increases from 27 to 1471 W. As a result, the value of the coefficient of performance of the heat pump increases from 0 to 0.9 for nitrogen gas.

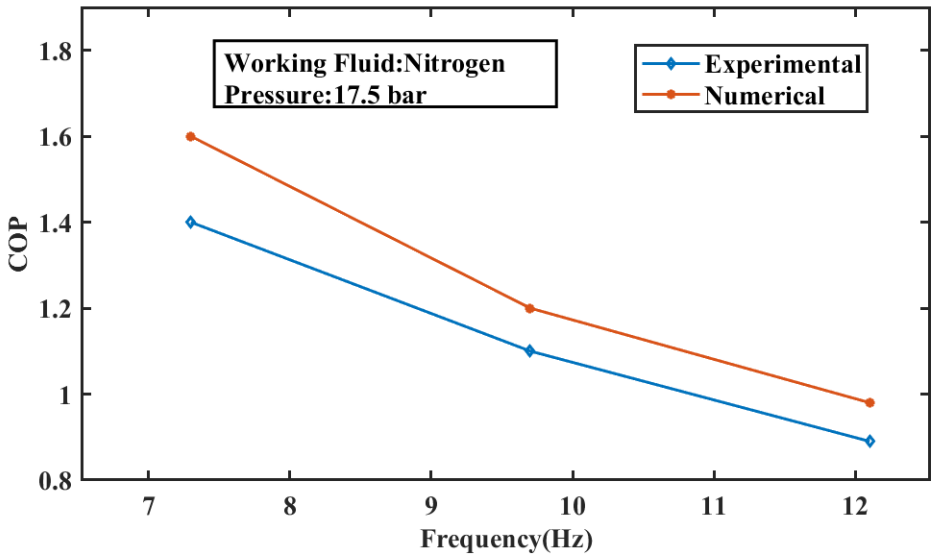

Figure 7: Validation of the model at different frequencies for heating

Table 3: Specification of FEMTO-60 engine as a heat pump [12]

No	Operating parameters	Value
1	Hot heat exchanger temperature	305K
2	Cold heat exchanger temperature	270K
3	Diameter of piston and displacer	60mm
4	Length of piston	62mm
5	Strokes of piston and displacer	40mm
6	Length of displacer	156mm
7	Length of regenerator	50mm
8	Diameter of regenerator	82mm
9	Wire diameter	112.00 µm
10	Porosity	0.64
11	Swept volume of compression space	$108cm^3$
12	Swept volume of expansion space	$113cm^3$
14	Working gas	Nitrogen
15	Frequency	5-13 Hz
16	Charging pressure	15-20 bar

Table 4: Validation of the current numerical model by engine model for Helium gas at $T_h = 977K$, $T_k = 288K$, $P_{mean} = 4.14MPa$, $f_r = 41.67Hz$

Model type	Output Power (W)	Error in power (%)	Efficiency	Error in efficiency (%)
Schmidt [33]	3455.00	42.77	70.70	230.99
Ideal adiabatic [32]	8300.00	242.97	62.30	193.43
Simple [10]	6700.00	176.86	52.50	146.48
CAF [16]	4107.00	69.71	36.90	69.95
Simple II [3]	3620.00	49.59	28.40	33.33
PSVL [5]	3030.00	25.21	24.40	14.55
PFST [17]	3611.00	49.21	23.30	9.39
CPMS [6]	2582.00	6.69	22.10	3.76
Non-Ideal 2nd order [31]	2659.00	9.88	20.40	5.92
Modified Simple [14]	2754.00	13.80	23.60	10.70
Current	**2640.00**	**9.10**	**20.24**	**6.10**
Experiment [25]	2420.00		21.30	

In this polytropic model, the two working spaces—known as the expansion and compression spaces—undergo polytropic processes. Consequently, we must determine the polytropic index of the gas in these working spaces to compute the polytropic heat transfer. Figure 6 shows the polytropic index as a function of the crank angle in both the compression and expansion space volumes. This polytropic index tends to be infinite at some points of crank angle due to simultaneous increases or decreases in pressure and a quasi-isochoric process when $dV \rightarrow 0$ (11). In addition, there is also some negative polytropic index at some points of the crank angle. This negative value may be due to the heat transfer and the transition point of the process from compression to expansion. During compression, the volume decreases while the pressure increases. However, if there is rapid heat transfer, the rate of pressure change exceeds the rate of volume change, resulting in a negative polytropic index. Similarly, during expansion, the volume increases while the pressure decreases. However, if the gas in the regenerator heats up rapidly, the increase in pressure as the volume increases leads to a negative polytropic index.

The developed numerical model is validated by comparing the experimental and numerical results at different frequencies, as shown in Figure 7. The temperature of the input water is about $9°C$ with a flow rate of 4 $L.min^{-1}$. The experimental result shows that the heat output is 1471 W after 90 minutes of operating time. The comparison of COP between the experimental conditions at 7.3, 9.7, and 12.1 Hz under 17.5 bar of nitrogen gas is shown in Fig.7. The experimental result shows that 0.89, 1.1, and 1.4 COP under 12.1, 9.7, and 7.3 Hz of frequency, respectively. The corresponding COP values are 0.9, 1.2, and 1.6 for numerical results. The relative errors for the experimental and numerical analysis are 1.1%, 9.0%, and 14.3% for the corresponding frequencies. Therefore, this result shows that the developed numerical model agrees with the experimental results. The heat pump's performance is reduced at higher frequencies, which may be due to an increase in mechanical friction loss, pressure drop work loss,

and gas spring hysteresis loss inside the heat pump.

The effect of charging pressure on the performance of the Stirling heat pump is shown in Fig.8. The performance of the heat pump increases with the increase in charging pressure. This result is expected due to the increase in the heat output of the heat pump. As pressure increases, the heat transfer of the power output from the heat exchanger increases in proportion to the increase in work input.

The variation of the polytropic heat transfer and shuttle heat loss is shown in Fig.9. The polytropic loss in the compression space is higher than the expansion space due to the maximum temperature of the working fluid inside the compression space.

Fig.10 shows how different working fluids influence the coefficient of performance of the Stirling heat pump as the operating frequency varies. The coefficients of performance of the Stirling heat pump using hydrogen and helium are higher than those of nitrogen and air within their operational frequency range. Compared to nitrogen and air, hydrogen and helium are lightweight, possess high thermal capacities, and have low molar masses, as shown in Table 5, which facilitates their flow through the different volumes of the heat pump (compression and expansion chambers, regenerator, heat exchangers). But at lower frequencies, nitrogen, air, and helium have almost the same performance.

Table 5: Thermophysical properties of different gases at 20°C and standard atmospheric pressure 101325 Pa [8, 19, 28, 34]

Gas	Dynamic viscosity μ (Pa·s)	Density ρ (kg·m^{-3})	Specific heat c_p (J·kg^{-1}·K^{-1})	Thermal conductivity λ (W·m^{-1}·K^{-1})	Adiabatic index γ	Molar mass $\mathcal{M}$ (kg·kmol^{-1})
Air	1.817	1.203	1015	0.02565	1.400	28.97
Helium	1.973	0.166	5196	0.14929	1.666	4.003
Hydrogen	0.867	0.084	14285	0.17690	1.410	2.016
Nitrogen	1.757	1.164	1040	0.02543	1.400	28.013

The comparison of the work losses at different frequencies in the Stirling heat pump for Nitrogen gases at a cooler and heater temperature of 270 K, 305 K, and 17.5 bar working pressure is shown in Fig.11. It is found that, especially at higher operating frequencies, the pressure drop work loss is the most prevalent of the four assessed loss mechanisms: mechanical friction loss, spring hysteresis loss, finite speed loss, and pressure drop loss. The increase in pressure drop work loss occurs because gas flows faster and with more turbulence through the regenerator and heat exchangers at higher frequencies, resulting in much higher flow resistance and pressure losses.

The comparison of the power losses at different frequencies in the Stirling heat pump for Nitrogen gases at a cooler and heater temperature of 270 K, 305 K, and 17.5 bar working pressure is shown in Fig.12. It is found that, especially at higher operating frequencies, the regenerator imperfection loss

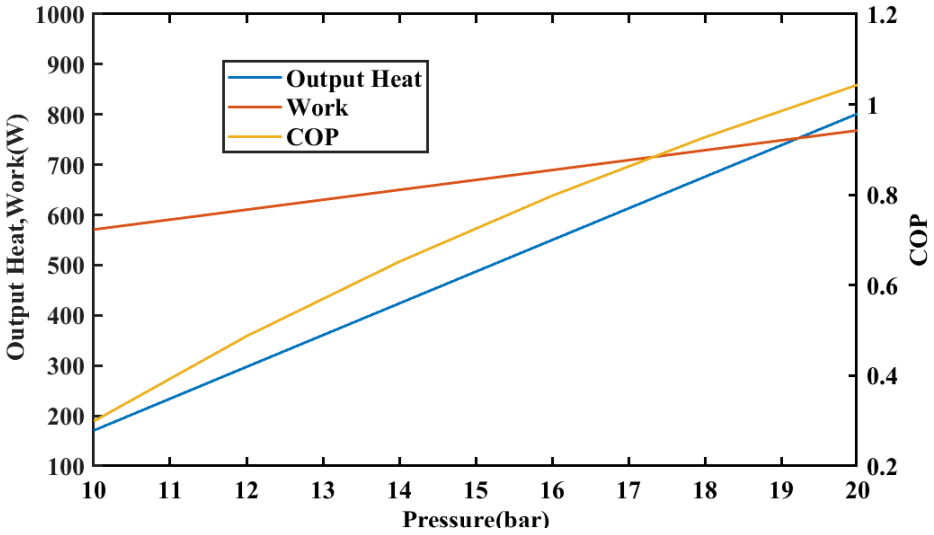

Figure 8: Effect of charging pressure at 725 rpm, 305 K, and 287 K, heater, and cooler temperature, respectively

is the most dominant loss of the five assessed loss mechanisms: regenerator imperfection loss, conduction heat loss, leakage heat loss, dissipation heat loss, and radiation heat loss. This loss increases significantly when the frequency rises because the residence time of the gas inside the regenerator decreases, which reduces the regenerator's effectiveness. This reduction in effectiveness leads to a reduction in regenerator imperfection loss in the heat pump regenerator. Radiation heat losses are very small and nearly constant, indicative of the small temperature difference (305–270 K) between heater and cooler.

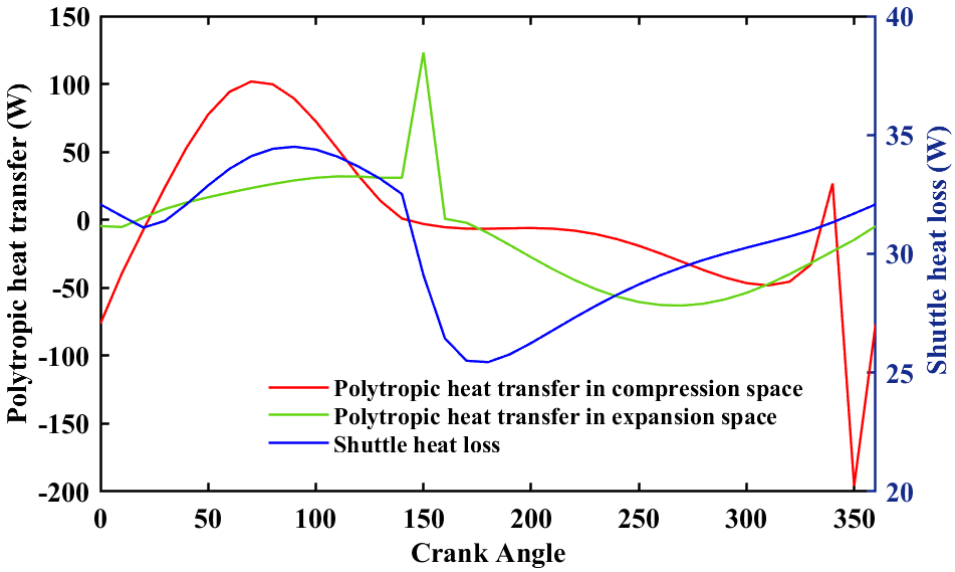

Figure 9: Variation of polytropic and shuttle heat loss in the cycle

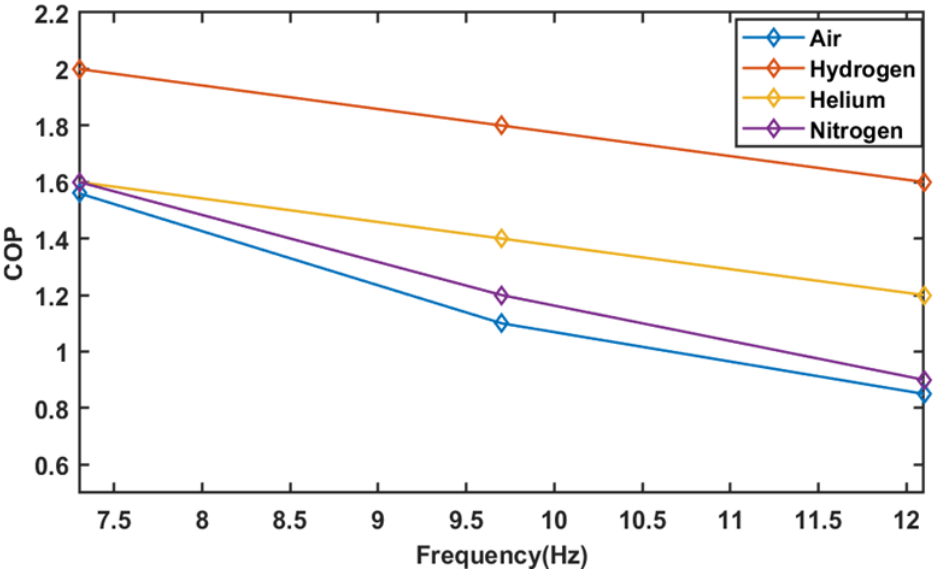

Figure 10: Influence of the frequency on the COP for different working gases at a cooler and heater temperatures of 270 K and 305 K, and 17.5 bar working pressure

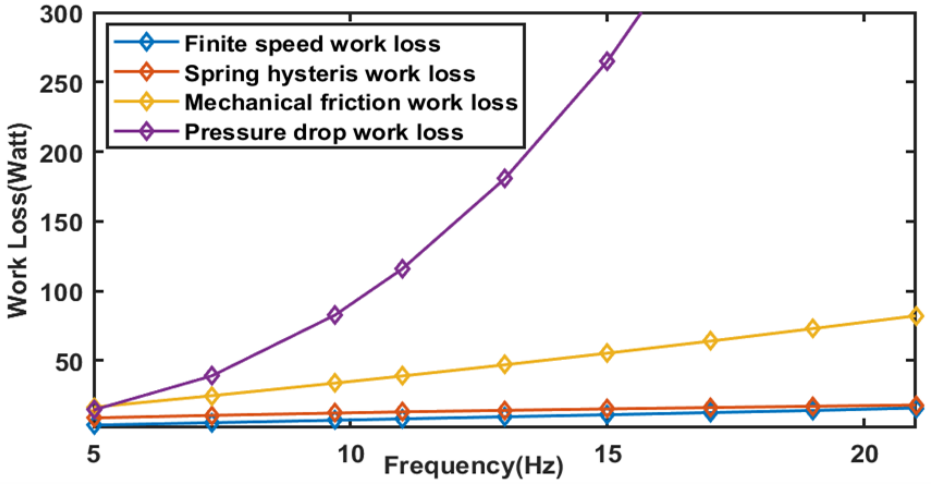

Figure 11: Influence of the frequency on the work loss for Nitrogen gas at a cooler and heater temperature of 270 K, 305 K, and 17.5 bar working pressure.

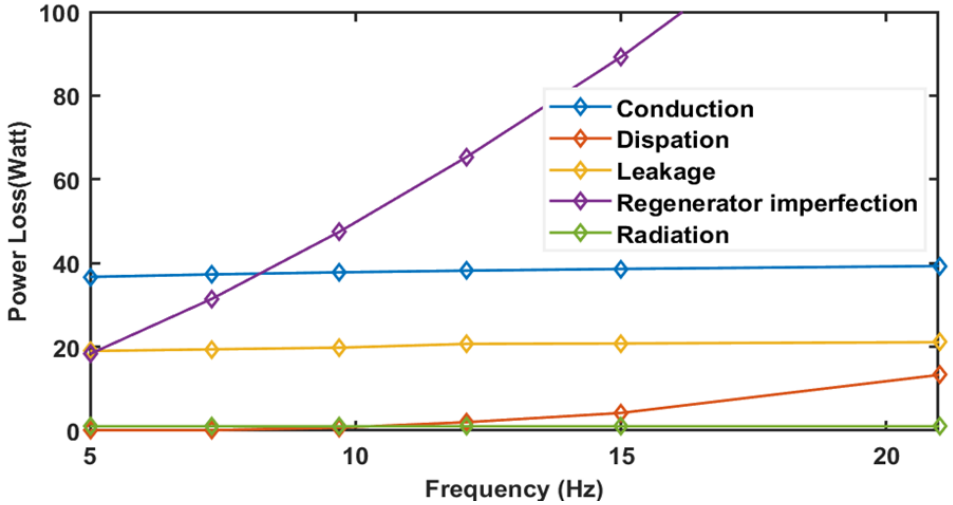

Figure 12: Influence of the frequency on the power loss for Nitrogen gas at a cooler and heater temperature of 270 K, 305 K, and 17.5 bar working pressure.

6. Conclusion

In this study, a new polytropic model called the new second-order Polytropic numerical model for the Stirling cycle heat pump has been developed to predict the performance of the Stirling heat pump. The developed numerical model is validated experimentally by changing the existing FEMTO-60 engine into a heat pump. The coefficient of performance (COP) predicted by the polytropic, adiabatic, and simple adiabatic thermodynamic models is compared to experimental results. The experimental result shows that 0.89, 1.1, and 1.4 COP under 12.1, 9.7, and 7.3 Hz of frequency, respectively. The corresponding COP values are 0.9, 1.2, and 1.6 for numerical results. The relative errors for the experimental and numerical analysis are 1.1%, 9.0%, and 14.3% for the corresponding frequencies.This result revealed that the polytropic model showed the closest agreement with the experimental results among them, indicating that it is better able to depict the behavior of Stirling heat pump systems. The error at lower frequencies is larger because of speed fluctuation.

We analyzed how the polytropic number varies with changes in expansion and compression space volume. We also examined how charging pressure, operating frequency, shuttle heat loss, polytropic heat transfer, power output, and work loss affect the heat pump's performance.

Furthermore, the effect of power and work loss in the Stirling heat pump has been investigated, and the result demonstrates that the pressure drop work loss in the heat exchanger and the regenerator imperfection losses are the two dominant losses in the heat pump. The radiation heat losses are very small and nearly constant, which is indicative of the very small temperature difference between heater and cooler, especially for heat pump and refrigeration systems, but in the case of the Stirling engine, this loss may increase due to a larger temperature difference between heater and cooler temperatures. Therefore, further optimization methods must be applied to the geometry of the regenerator to reduce these two dominant losses, and the numerical model developed must be experimentally validated for different working fluids (like Helium and Hydrogen) to improve the reliability of the model.

Declaration of competing interest

The authors declare that they have no known competing financial interests or personal relationships that could have appeared to influence the work reported in this paper.

Acknowledgments

This work has been supported by the EIPHI Graduate School (contract ANR-17-EURE-0002) and the Université Marie et Louis Pasteur, the Embassy of France to Ethiopia, the African Union, and the Ministry of Educa-

tion of Ethiopia.

References

[1] Fawad Ahmed, Huang Hulin, and Aqib Mashood Khan. Numerical modeling and optimization of beta-type stirling engine. *Applied Thermal Engineering*, 149:385–400, 2019.

[2] Suliman Alfarawi, Raya Al-Dadah, and Saad Mahmoud. Enhanced thermodynamic modelling of a gamma-type stirling engine. *Applied Thermal Engineering*, 106:1380–1390, 2016.

[3] Mojtaba Babaelahi and Hoseyn Sayyaadi. Simple-ii: a new numerical thermal model for predicting thermal performance of stirling engines. *Energy*, 69:873–890, 2014.

[4] Mojtaba Babaelahi and Hoseyn Sayyaadi. Modified psvl: a second order model for thermal simulation of stirling engines based on convective–polytropic heat transfer of working spaces. *Applied Thermal Engineering*, 85:340–355, 2015.

[5] Mojtaba Babaelahi and Hoseyn Sayyaadi. A new thermal model based on polytropic numerical simulation of stirling engines. *Applied Energy*, 141:143–159, 2015.

[6] Mojtaba Babaelahi and Hoseyn Sayyaadi. Analytical closed-form model for predicting the power and efficiency of stirling engines based on a comprehensive numerical model and the genetic programming. *Energy*, 98:324–339, 2016.

[7] William T Beale. Stirling cycle type thermal device, January 5 1971. US Patent 3,552,120.

[8] Sydney Chapman and Thomas George Cowling. *The mathematical theory of non-uniform gases: an account of the kinetic theory of viscosity, thermal conduction and diffusion in gases*. Cambridge university press, 1990.

[9] SC Costa, Harritz Barrutia, Jon Ander Esnaola, and Mustafa Tutar. Numerical study of the pressure drop phenomena in wound woven wire matrix of a stirling regenerator. *Energy Conversion and Management*, 67:57–65, 2013.

[10] M Costea, S Petrescu, and C Harman. The effect of irreversibilities on solar stirling engine cycle performance. *Energy conversion and management*, 40(15-16):1723–1731, 1999.

[11] Zhang Cun-Quan, Wu Yi-Nong, Ji Guo-Lin, Liu Dong-Yu, and Xu Lie. Dynamic simulation of one-stage oxford split-stirling cryocooler and comparison with experiment. *Cryogenics*, 42(9):577–585, 2002.

[12] S. Djetel-Gothe, S. Bégot, F. Lanzetta, and E. Gavignet. Design, manufacturing and testing of a beta stirling machine for refrigeration applications. *International Journal of Refrigeration*, 115:96–106, 2020.

[13] David Gedeon and JG Wood. Oscillating-flow regenerator test rig: hardware and theory with derived correlations for screens and felts. Technical report, 1996.

[14] Muluken Zegeye Getie. *Numerical modeling and optimization of a regenerative Stirling refrigerating machine for moderate cooling applications*. PhD thesis, Université Bourgogne Franche-Comté, 2021.

[15] Vlad Mario Homutescu, G Dumitrascu, and Bogdan Horbaniuc. Evaluation of the work lost due to leaks through cylinder-displacer gap. *COFRET Nantes*, 2(1):70–74, 2008.

[16] Hadi Hosseinzade and Hoseyn Sayyaadi. Cafs: The combined adiabatic–finite speed thermal model for simulation and optimization of stirling engines. *Energy conversion and Management*, 91:32–53, 2015.

[17] Hadi Hosseinzade, Hoseyn Sayyaadi, and Mojtaba Babaelahi. A new closed-form analytical thermal model for simulating stirling engines based on polytropic-finite speed thermodynamics. *Energy conversion and management*, 90:395–408, 2015.

[18] William Morrow Kays and Alexander Louis London. Compact heat exchangers. 1984.

[19] J Kestin, K Knierim, EA Mason, B Najafi, ST Ro, and M Waldman. Equilibrium and transport properties of the noble gases and their mixtures at low density. *Journal of physical and chemical reference data*, 13(1):229–303, 1984.

[20] Jacob Wl Kohler. The stirling refrigeration cycle in cryogenic technology. *Adv. Sci.*, 25:261, 1968.

[21] Ruijie Li and Lavinia Grosu. Parameter effect analysis for a stirling cryocooler. *International Journal of Refrigeration*, 80:92–105, 2017.

[22] Ruijie Li, Lavinia Grosu, and Wei Li. New polytropic model to predict the performance of beta and gamma type stirling engine. *Energy*, 128:62–76, 2017.

[23] M Mahmoodi, J Pirkandi, and A Alipour. Numerical simulation of beta type stirling engine considering heat and power losses. *Iranian Journal of Mechanical Engineering Transactions of the ISME*, 15(2):5–27, 2014.

[24] Nadia Martaj, Lavinia Grosu, and Pierre Rochelle. Thermodynamic study of a low temperature difference stirling engine at steady state operation. *International Journal of Thermodynamics*, 10(4):165–176, 2007.

[25] William R Martini. Stirling engine design manual. Technical report, 1983.

[26] Temesgen Assefa Minale, François Lanzetta, Sylvie Bégot, and Muluken Z Getie. Review on the technological advancement of stirling cycle heat pumps. *Energy Reports*, 12:3504–3518, 2024.

[27] Temesgen Assefa Minale, Francois Lanzetta, Sylvie Begot, and Muluken Z Getie. *Thermodynamics Modeling and Optimization of Stirling Heat Pump: A Review*, pages 289–306. Springer Nature Switzerland, Cham, 2024.

[28] Bruce E Poling, John M Prausnitz, O'Connell John Paul, and Robert C Reid. *The properties of gases and liquids*, volume 5. Mcgraw-hill New York, 2001.

[29] Johannes M Strauss and Robert T Dobson. Evaluation of a second order simulation for sterling engine design and optimisation. *Journal of Energy in Southern Africa*, 21(2):17–29, 2010.

[30] Youssef Timoumi, Iskander Tlili, and Sassi Ben Nasrallah. Design and performance optimization of gpu-3 stirling engines. *Energy*, 33(7):1100–1114, 2008.

[31] Godfrey T Udeh, Stavros Michailos, Derek Ingham, Kevin J Hughes, Lin Ma, and Mohammed Pourkashanian. A new non-ideal second order thermal model with additional loss effects for simulating beta stirling engines. *Energy Conversion and Management*, 206:112493, 2020.

[32] Israel Urieli. Stirling cycle machine analysis. 2020.

[33] Israel Urieli and David M Berchowitz. Stirling cycle engine analysis. 1984.

[34] Gordon J Van Wylen, Richard E Sonntag, and Claus Borgnakke. *Fundamentals of classical thermodynamics*. Wiley, 1994.

[35] Chih Wu. Recent advances in finite-time thermodynamics. 1999.